Concrete Science and Engineering, Vol. 4, June 2002, pp 106-113

RESEARCH PAPERS

Reactivity of fly ash: extension and application of a shrinking core model

H. J. H. Brouwers and R. J. van Eijk
Department of Civil Engineering, University of Twente, P.O. Box 217, 7500 AE Enschede, The Netherlands

ABSTRACT

In the present paper a theoretical study is presented on the dissolution (reaction) of pulverised powder coal fly ash. A shrinking core model is derived for hollow spheres that contain two regions (outer hull and inner region). The resulting analytical equations are applied to the dissolution experiments by Pietersen [1, 2], yielding reaction rates at various temperatures and pH for two class F fly ashes, that are separated in solid spheres and in hollow cenospheres. It is revealed that the available amount of reactive fly ash is proportional to the glass content of the fly ash, and that the reaction rate is proportional to this glass content as well. Moreover, it is concluded that the outer region is less reactive than the inner region, and that these reactivities are proportional to a power of the hydroxyl concentration. Subsequently, experimental data and model are used to assess the magnitude of inner and outer region. It seems that the outer hull of solid spheres and cenospheres are having the same thickness, about 2 µm.

1. INTRODUCTION

In the use and production of cement and concrete nowadays more and more secondary materials are employed such as pulverised coal fly ash, granulated blast furnace slag and silica fume. These products exhibit hydraulic or pozzolanic behaviour, *i.e.* they are able to react with water or water-dissolved calcium hydroxide (CH), respectively, to form pozzolanic C-S-H, a cement hydration product.

It is understood that the ability of secondary materials to react strongly depends on the alkali content and temperature of the water [3-8]. To investigate this, Pietersen [1, 2] performed pulverised coal fly ash dissolution experiments. During these experiments several pulverised fly ashes were dissolved in sodium hydroxide solutions of pH 13, 13.4 and 13.7, at various temperatures. As expected, dissolution rates (and, as one might expect: related reaction rates as well) increased significantly with increasing pH and temperature.

As said, the relation between reaction rate at one hand and pH and temperature on the other hand has been mentioned by several authors. However, to the authors' knowledge, no analytical relation has been derived between reaction rate and pH and temperature. As this is of major importance to understand the hydration of cements blended with said secondary raw materials, in this paper addresses such a relation is derived and applied.

First, a comprehensive model is presented of the dissolution of a sphere, using a shrinking core model approach as first proposed by Yagi and Kunii [9]. Here, the sphere is allowed to be hollow (to account for cenospheres) and to consist of two (concentric) regions (to account for different composition and reactivity). Subsequently, the resulting equations are applied to the experiments of Pietersen [1, 2]. Based on this application, magnitude and reactivities of outer region (outer hull) and inner region are assessed.

2. EXPERIMENTS

Pietersen [1, 2] has reported dissolution experiments with two different class F fly ashes ("EFA" and "LM") at pH = 13, 13.4 and 13.7. The dissolution experiments were executed at temperatures of 20°C, 30°C and 40°C. Sodium hydroxide (NaOH) was chosen as reaction medium and each time 100 mg of fly ash was reacted with 100 ml of solution in sealed plastic bottles. Actually, the OH^- concentration (thus pOH) has been imposed, and the pH been determined via pH + pOH = 14 [10]. However, this relation is applicable only in case the temperature is 20°C and hence, here the pOH is used henceforth.

ISSN 1295-2826/02

The two fly ashes originate from two different power plants and have broad and mutually different particle size distributions. One power plant was a "wet-bottom" type plant that operates at 1800°C (EFA); the other FA originates from a low NO_x furnace plant (LM).

All dissolution experiments where executed with a sieved part of the fly ashes, the diameter lying between 38 µm and 50 µm. The fly ashes have also been ultrasonically vibrated to prevent agglomeration of small particles to large ones. In Table 1 the most important properties of both fly ashes are summarised. In this table also the crystalline SiO_2 and Al_2O_3 that are part of the mullite are specified, using the molar masses of both substances (M_A = 102 g/mole, M_S = 60 g/mole) and considering that mullite contains (by mass) 306/426 Al_2O_3 and 120/426 silica.

For the dissolution experiments the particles were separated into a fraction of low density ("cenospheres") with a density smaller than 1400 kg/m^3 and in a fraction of high density ("solid spheres") with a density of 2300-2600 kg/m^3. SEM images of polished sections of these fractions revealed that the cenospheres were hollow thin-walled spheres. Dissolution experiments were also executed with the hollow cenospheres and the solid spheres, which differ in density about a factor of two [1, 2].

The experiments revealed that for these two fly ashes Si, Al and K all congruently dissolve, implying bulk dissolution. Accordingly, the dissolution of one component, Si, represents an adequate measure for the dissolution of the entire glass mass. This principle was used for the experiments which are used here.

In Figs. 1 and 2 the fraction of the mass dissolved (z) is depicted against time for EFA and LM solid spheres, respectively, for three pOH levels and at 40°C. One can readily see that all experiments show a similar path in time, and that at lower pOH (larger OH^- concentration) the removal is largest. Images of leached particles revealed the creation of a hollow structure originating from the leached glass phase with remains of needle shape inert (crystalline) material. This finding is in agreement with etching experiments by Hulett and Weinberger [11] and by Hemmings and Berry [12].

In Figs. 3 and 4 the mass dissolved from cenospheres and solid spheres for EFA and LM, respectively, are depicted at pOH = 0.3 and 40°C. In Figs. 5 and 6 the dissolution of solid spheres for EFA and LM, respectively, are set out for 20°C, 30°C and 40°C and at pOH = 0.3. One can see that cenospheres dissolve faster, and that higher temperature enhance the dissolution rate.

In the subsequent section a model is derived which adequately describes the dissolution experiments. The

Table 1 – Composition (in m/m %) of investigated fly ashes [2], specification of crystalline SiO_2 and Al_2O_3 in mullite (all percentages based on total fly ash mass)

	EFA		LM	
	solid	ceno	solid	ceno
Overall composition				
SiO_2	55.56%	51.55%	57.39%	52.21%
Al_2O_3	27.39%	31.96%	31.18%	39.54%
Fe_2O_3	4.65%	2.96%	3.50%	2.02%
TiO_2	1.20%	0.91%	1.90%	1.43%
MgO	1.82%	1.41%	0.28%	0.24%
CaO	2.83%	0.80%	2.75%	1.15%
Na_2O	1.84%	1.94%	0.37%	0.38%
K_2O	4.40%	5.68%	1.00%	1.02%
P_2O_5	n.d.	n.d.	0.54%	n.d.
H_2O	0.3%	0.4%	1.1%	1.4%
LOI (carbon)	0.0%	2.4%	0.0%	0.6%
Of which:				
mullite ($3Al_2O_3 \cdot 2SiO_2$)	2.1%	5.4%	20.5%	36.2%
quartz (SiO_2)	3.0%	3.0%	12.8%	1.6%
	------	-------	---------	---------
total crystalline	5.1%	8.4%	33.3%	37.8%
non-crystalline (ϕ)	94.9%	6%	66.7%	62.2%
Hence				
SiO_2 in mullite	0.6%	1.5%	5.8%	10.2%
Al_2O_3 in mullite	1.5%	3.9%	14.7%	26.0%

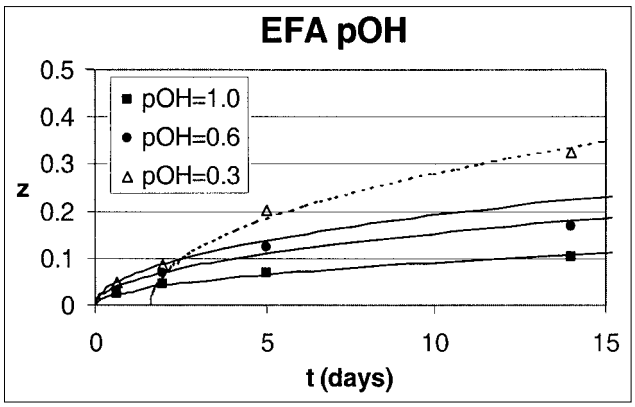

Fig. 1 – Fraction of mass dissolved z versus time [2] and fit (Equations (31) and (32)) for EFA solid spheres (b = 1) at pOH = 0.3, 0.6 and 1 (T = 40°C).

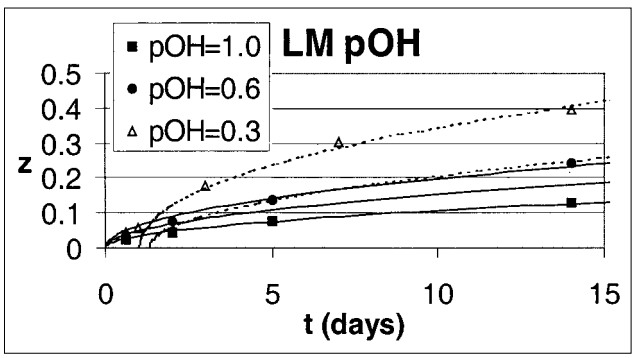

Fig. 2 – Fraction of mass dissolved z versus time [2] and fit (Equations (31) and (32)) for LM solid spheres (b = 1) at pOH = 0.3, 0.6 and 1 (T = 40°C).

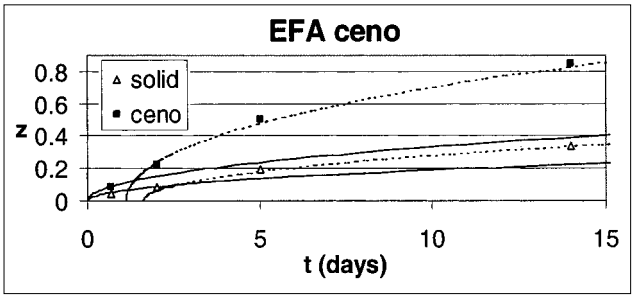

Fig. 3 – Fraction of mass dissolved z versus time [2] and fit (Equations (31) and (32)) for EFA cenospheres (b = 0.5) and solid spheres (pOH = 0.3, T = 40°C).

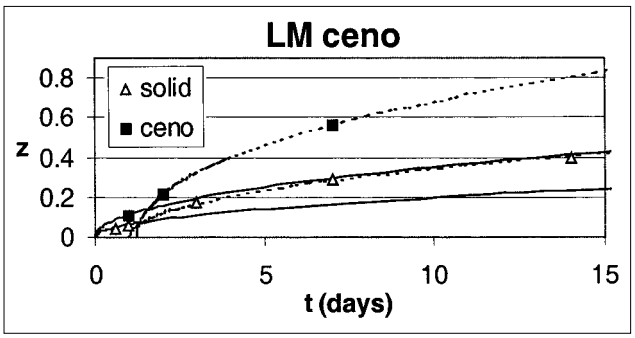

Fig. 4 – Fraction of mass dissolved z versus time [2] and fit (Equations (31) and (32)) for LM cenospheres (b = 0.5) and solid spheres (pOH = 0.3, T = 40°C).

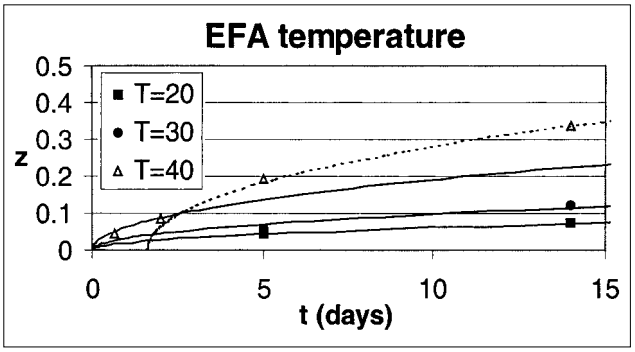

Fig. 5 – Fraction of mass dissolved z versus time [2] and fit (Equations (31) and (32)) for EFA solid spheres at T = 20°C, 30°C and 40°C (pOH = 0.3).

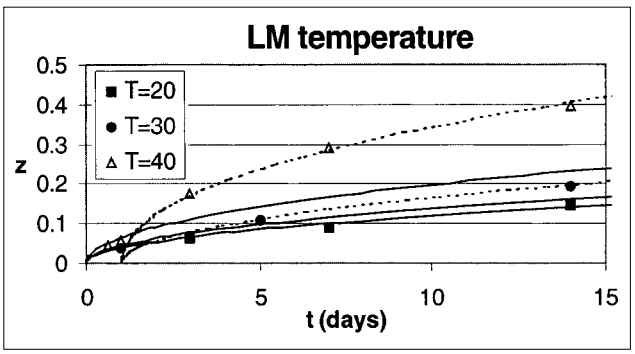

Fig. 6 – Fraction of mass dissolved z versus time [2] and fit (Equations (31) and (32)) for LM solid spheres at T = 20°C, 30°C and 40°C (pOH = 0.3).

observation of a removed glass phase and an inert crystalline phase suggests the application of a shrinking core model [9, 13]. Furthermore, the trend of the dissolved mass versus time suggests a control by diffusion through the dissolved shell.

3. DISSOLUTION MODEL EQUATIONS

In this section the dissolution of a spherical particle in an infinite large liquid volume is modelled. This particle is considered to be spherical, and to have a phase that dissolves and leaves porosity, and an inert part that is unaffected. In fly ash and slag the dissolving part corresponds to the glass phase, whereas the inert part can be thought of as the crystalline inert phase. The unreacted core shrinks, and the dissolved glass diffuses through the porous shell of inert material towards the solvent. Therefore, the part of the volume that is dissolving is named porosity ϕ and hence the inert part $1 - \phi$. This shrinking unreacted core model was first presented by Yagi and Kunii [9] and an extensive treatment can be found in Levenspiel [13]. Here, this model will be applied on the leaching of glass from fly ash assuming control by diffusion through the dissolved shell, following the treatment of Levenspiel [13]. The model presented here differs in two aspects from the conventional model:

1. Here we permit the sphere to be hollow, as is the case in cenospheres. From analyses by among others Pietersen [1, 2], Hemmings and Berry [12] it follows that some fly ash particles have a hollow core, which results in a lower mean density of these cenospheres. Some particles are really completely hollow, while other particles also contain material inside the hollow core (other solid and/or hollow particles). Here it is assumed that the outer enclosing wall will be sufficiently thick so that a breakthrough of this wall will not occur. Accordingly, the particle can be modelled as a completely hollow sphere.

2. From Figs. 1-6 it follows that for glass removal rates up to about 20% the experiments follow a path which can be explained with a diffusion rate limited shrinking core model. For higher removal rates (appearing at higher OH^- concentrations and/or higher temperature), however, it seems that glass removal accelerates. Accordingly, here the sphere is considered to consist of two regions, the interior glass and the exterior glass, a concept that is also mentioned by Hemmings and Berry [12].

Hence, consider a hollow spherical particle with an inner radius r_h and an outer radius R and an external surface A. The particle possesses an outer and an inner

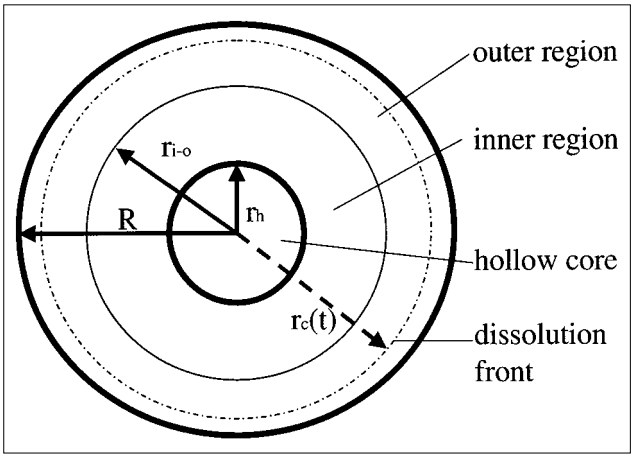

Fig. 7 – Schematic representation of dissolving hollow sphere containing two regions.

region, the boundary between both regions designated as $r_{i\text{-}o}$ and the reacting surface designated as r_c (Fig. 7).

In an alkali environment, OH^- ions are diffusing towards the reacting surface, whereas released glass ions (SiO_3^{2-} and others such as AlO_2^-) are diffusing from glass core to the surrounding liquid. Both SiO_2 and Al_2O_3 are the major constituents of the glass (Table 1) and are hydrated to aforesaid ions for pH larger than about 12 [14, 15]. As the silica release has been measured by Pietersen [1, 2], here the release of this constituent is focused on. For all other constituents a similar analysis can be performed.

The steady-state diffusion equation for SiO_3^{2-} ion diffusing through the leached shell now reads:

$$\frac{d(r^2 D_e \frac{dC_S}{dr})}{dr} = 0 \tag{1}$$

The effective diffusion coefficient depends on the ion concentrations [16] and on the porosity of the leached shell [17]. When the concentration of one ion is smaller than the other, the effective diffusion coefficient takes the value of that ion present in smaller concentration [16]. Here it is assumed that the concentration of the SiO_3^{2-} ion is much smaller than the OH^- concentration, so that D_e is constant. The effective diffusion coefficient in the porous shell is related to the bulk diffusion coefficient via Archie's law [17]:

$$D_{e\,S} = \phi^a D_S \tag{2}$$

The parameter a varies between 1.5 and 2.5, here a value of 2 is imposed, which is also recommended by Wakao and Smith [18]. The boundary conditions of Equation (1) read:

$$C_S(r = R) = 0 \tag{3}$$

$$C_S(r = r_c) = C_{Sc} \tag{4}$$

The first condition reflects the negligible small SiO_3^{2-} concentration in the surrounding liquid, whereas the second boundary condition states the SiO_3^{2-} concentration at the glass core.

Solving Equations (1), (3) and (4) yields:

$$C_S(r) = \left[\frac{C_{Sc} r_c}{R - r_c}\right]\left[\frac{R}{r} - 1\right] \tag{5}$$

The SiO_3^{2-} molar flux from the glass surface now reads:

$$\dot{m}_S = -D_{eS}\frac{dC_S}{dr}\bigg|_{r_c} = \frac{D_{eS} C_{Sc} R}{(R - r_c) r_c} \tag{6}$$

The silica decrease of the particle by dissolution now reads:

$$\phi x_S \rho_g \frac{4\pi}{3}\frac{dr_c^3}{dt} = -A_c \dot{m}_S \tag{7}$$

in which ρ_g is the molar density of the glass and x_S its mole fraction of silica and whereby $\dot{m}_S$ follows from Equation (6). Inserting

$$A_c = 4\,\pi\, r_c^2 \tag{8}$$

and introducing:

$$r^* = \frac{r}{R} \tag{9}$$

$$\tau = \frac{x_S \rho_g R^2}{6\phi D_S C_{Sc}} \tag{10}$$

in which Equation (2) has been substituted, yields the following first order ordinary differential equation for the dimensionless radius:

$$\frac{dr_c^*}{dt}(r_c^* - 1) r_c^* = \frac{1}{6\tau} \tag{11}$$

With as initial condition:

$$r_c^*(t = 0) = 1 \tag{12}$$

in case the outer region is considered, and:

$$r_c^*(t = t_{i-o}) = r_{i-o}^* \tag{13}$$

when the dissolution of the inner region is considered. Note that τ is different for the inner and outer regions, which are therefore denoted by τ_i and $\tau_{o,}$, respectively.

4. SOLUTION OF MODEL EQUATIONS

In this section the derived equation of the previous section are solved in closed-form. Integrating Equation (11) and application of Equations (12) and (13) yields, respectively:

$$t = (1 - 3r_c^{*2} + 2r_c^{*3})\tau_o \tag{14}$$

$$t = (3r_{i-0}^{*2} - 2r_{i-o}^{*3} - 3r_c^{*2} + 2r_c^{*3})\tau_i + t_{i-o} \tag{15}$$

which are both implicit relations of r^* as a function of time. Note that r_{i-0}^* and t_{i-o}, using Equation (14), are related by:

$$t_{i-o} = (1 - 3r_{i-0}^{*2} + 2r_{i-o}^{*3})\tau_o \tag{16}$$

Substituting this equation into Equation (15) produces:

$$t = (1 - 3r_c^{*2} + 2r_c^{*3})\tau_i + t_{i-o}(1 - \frac{\tau_i}{\tau_o}) \tag{17}$$

for the inner region.

Here distinction has been made between an outer and inner region which may have among others different porosity (glass fraction), glass molar density and glass silica content. Often, also by Pietersen [1, 2], average values are given, such as the conversion factor. Hence, the expressions derived here will be related to average particle quantities.

The mean glass density of the particle is related to the properties of inner and outer region via:

$$\overline{\phi\rho_g}(R^3 - r_h^3) = \phi_o\rho_{go}(R^3 - r_{i-o}^3) + \phi_i\rho_{gi}(r_{i-o}^3 - r_h^3) \tag{18}$$

Similarly, the average glass silica content is related to the contents in outer and inner region via:

$$\begin{aligned}\overline{x_S\phi\rho_g}(R^3 - r_h^3) = {} & x_{So}\phi_o\rho_{go}(R^3 - r_{i-o}^3) \\ & + x_{Si}\phi_i\rho_{gi}(r_{i-o}^3 - r_h^3)\end{aligned} \tag{19}$$

The glass mass removed (or, conversion factor) for the outer region reads:

$$z = 1 - \frac{\phi_o\rho_{go}(r_c^3 - r_{i-o}^3) + \phi_i\rho_{gi}(r_{i-o}^3 - r_h^3)}{\overline{\phi\rho_g}(R^3 - r_h^3)} \tag{20}$$

Analogously, the fraction of glass silica dissolved (or, silica conversion factor) for the outer region follows from:

$$z_S = 1 - \frac{x_{So}\phi_o\rho_{go}(r_c^3 - r_{i-o}^3) + x_{Si}\phi_i\rho_{gi}(r_{i-o}^3 - r_h^3)}{\overline{x_S\phi\rho_g}(R^3 - r_h^3)} \tag{21}$$

Combining Equations (18) and (20) and Equations (19) and (21) reveals:

$$z_S = z\frac{x_{So}}{x_S} \tag{22}$$

The glass conversion rate of the inner region reads:

$$z = 1 - \frac{\phi_i\rho_{gi}(r_c^3 - r_h^3)}{\overline{\phi\rho_g}(R^3 - r_h^3)} \tag{23}$$

and the silica conversion rate for the inner region is:

$$z_S = 1 - \frac{x_{Si}\phi_i\rho_{gi}(r_c^3 - r_h^3)}{\overline{x_S\phi\rho_g}(R^3 - r_h^3)} \tag{24}$$

Combining Equations (23) and (24) reveals that for the inner region holds:

$$1 - z_S = (1 - z)\frac{x_{Si}}{x_S} \tag{25}$$

Note that Equation (20) coincides with Equation (23) and Equation (22) with Equation (24) for $r_c = r_{i-o}$ (*i.e.* on the transition of inner and outer region), as would be expected.

In order to express r_c in to z and z_S, Equation (21) is rewritten by inserting Equation (19) in the nominator and introducing b (which can be seen as is the ratio between apparent mean density of the hollow sphere and the mean glass density):

$$b = \frac{\rho_a}{\rho_g} = 1 - \frac{r_h^3}{R^3} = 1 - r_h^{*3} \tag{26}$$

yielding for the outer region:

$$r_c^{*3} = 1 - z_S b\frac{\overline{x_S\phi\rho_g}}{x_{So}\phi_o\rho_{go}} = 1 - zb\frac{\overline{\phi\rho_g}}{\phi_o\rho_{go}} \tag{27}$$

see Equations (9) and (22). Substituting Equations (19) and (26) into Equation (23) yields for the inner region:

$$r_c^{*3} = 1 - b + (1 - z_S)b\frac{\overline{x_S\phi\rho_g}}{x_{Si}\phi_i\rho_{gi}} = 1 - b + (1 - z)b\frac{\overline{\phi\rho_g}}{\phi_i\rho_{gi}} \tag{28}$$

see Equations (9) and (25). Equations (27) and (28) can be combined with Equations (14) and (17), respectively, yielding:

$$t = (1 - 3(1 - z_S b\frac{\overline{x_S\phi\rho_g}}{x_{So}\phi_o\rho_{go}})^{\frac{2}{3}} + 2(1 - z_S b\frac{\overline{x_S\phi\rho_g}}{x_{So}\phi_o\rho_{go}}))\tau_o \tag{29}$$

$$\begin{aligned}t = {} & (1 - 3(1 - b + (1 - z_S)b\frac{\overline{x_S\phi\rho_g}}{x_{Si}\phi_i\rho_{gi}})^{\frac{2}{3}} \\ & + 2(1 - b + (1 - z_S)b\frac{\overline{x_S\phi\rho_g}}{x_{Si}\phi_i\rho_{gi}}))\tau_i + t_{i-o}(1 - \frac{\tau_i}{\tau_o})\end{aligned} \tag{30}$$

Note that Equations (27) and (28) become identical when the spheres are homogeneous, *i.e.* when

$\overline{x_S \phi \rho_g} = x_{So} \phi_o \rho_{go} = x_{Si} \phi_i \rho_{gi}$ and that equations (29) and (30) then reduce to:

$$t = (1 - 3(1 - zb)^{\frac{2}{3}} + 2(1 - zb))\tau_o \quad (31)$$

$$t = (1 - 3(1 - zb)^{\frac{2}{3}} + 2(1 - zb))\tau_i + t_{i-o}(1 - \frac{\tau_i}{\tau_o}) \quad (32)$$

Furthermore, note that for $\tau_i = \tau_o$ (see Equation (10)), Equations (31) and (32) are identical, in case of solid spheres (b = 1) they furthermore reduce to the common shrinking core model expressions.

In Fig. 8a z is depicted against t for b = 1 (massive spheres) using Equations (31) and (32). As example, τ_o has been set equal to 30 s., τ_i to 10 s. and t_{i-o} $(1-\tau_i/\tau_o)$ to 3 s., *i.e.* a case whereby the inner region is more reactive than the outer region.

One can readily see that for $\tau_i < \tau_o$ the glass removal line crosses the horizontal axis at t > 0 and climbs steeper in time. This behaviour was also seen in Figs. 1-6, implying two regions with two different τ. In the following section Equations (31) and (32) are applied to the experimental data depicted in said Figures. In Fig. 8b a case whereby the inner region is less reactive than the outer region is depicted, τ_o has been set equal to 10 s., τ_i to 30 s. and t_{i-o} $(1-\tau_i/\tau_o)$ to - 3 s. One can see that when the inner region is attained, removal proceeds slower.

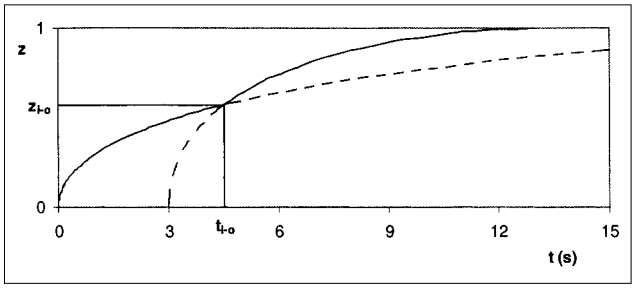

Fig. 8a – Mass removal versus time for a solid sphere (b = 1) using Equations (31) and (32), τ_o = 30 s, τ_i = 10 s. and t_{i-o} $(1-\tau_i/\tau_o)$ = 3 s.

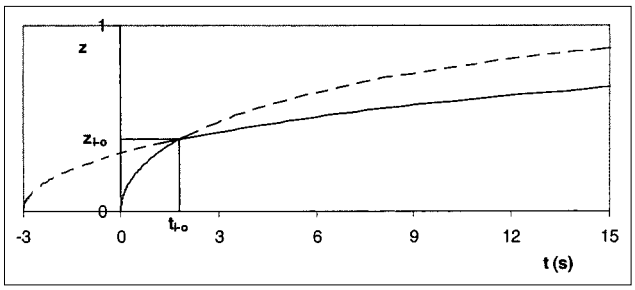

Fig. 8b – Mass removal versus time for a solid sphere (b = 1) using Equations (31) and (32), τ_o = 10 s, τ_i = 30 s. and t_{i-o} $(1-\tau_i/\tau_o)$ = -3 s.

5. MODEL APPLICATION

In Figs. 1-6 Equation (31) has been fitted to the experimental data by adapting τ_o. For the solid spheres b has been set equal to unity, whereas for the cenospheres b equals 0.5 [1, 2]. Furthermore, it has been assumed a priori that the silica is homogeneously distributed, *i.e.* $\overline{x_S \phi \rho_g} = x_{So} \phi_o \rho_{go} = x_{Si} \phi_i \rho_{gi}$ and hence, $z = z_S$ (the fraction of removed glass is identical to fraction of removed silica, this latter quantity was measured by Pietersen [1, 2]). When the inner region has been reached, *i.e.* when Equation (31) is not able to match the measured removal rates anymore (at larger t), Equation (32) was fitted to these data by adapting τ_i.

From Figs. 1-6 it follows that for the solid spheres the inner region is attained when about 7% (LM) to 9% (EFA) of the silica/glass has been dissolved (= $z_{i-o} = z_{Si-o}$). Said values imply that the boundary between both regions is located at about 96-97% of the external radius of the sphere. These values are identical for all experiments, regardless the pOH and temperature of the experiment. At higher pH and higher temperature the lines intersect after 1-2 days (= t_{i-o}), whereas for low temperatures even after 15 days the – more reactive – inner region has not been attained yet. For the cenospheres, Figs. 3 and 4 learn that the outer region comprises 12% (EFA) to 13% (LM) of sphere mass. As b = 0.5 (and hence $r_h^{*3} = 0.80$, see Equation (26)), the inner core mass of cenospheres is effectively reduced by about 50% in comparison to solid spheres, it can be concluded that the thickness of the outer layer of hollow spheres is the same (for LM) or a little thinner (EFA) than for their solid counterparts, and amounts about 2 μm as d = 38–50 μm. Note that this outer hull comprises about half of the thickness of the cenosphere wall: 0.2 x (38–50 μm)/2 = 3.8–5 μm.

For each set of experimental data the best τ has been chosen at first sight. In Tables 2-7 the assessed values of τ have been listed for all experiments. One can see that the reaction time τ decreases, *i.e.* increasing reactivity, with increasing hydroxide concentration and temperature

Table 2 – Reaction time τ for various pOH and [OH⁻] for EFA solid spheres (T = 40°C) assuming $\overline{x_S} / x_{Si} = 1$ and $\overline{x_S} / x_{So} = 1$

pOH	[OH⁻] (mole/l)	τ_o (days)	τ_i (days)	$t_{i-o}(1-\tau_i/\tau_o)$ (days)
1.0	0.100	3500		
0.6	0.251	1200		
0.3	0.501	750	275	1.6

Table 3 – Reaction time τ for various pOH and [OH^-] for LM solid spheres (T = 40°C) assuming $\overline{x_S} / x_{Si} = 1$ and $\overline{x_S} / x_{So} = 1$

pOH	[OH^-] (mole/l)	τ_o (days)	τ_i (days)	$t_{i\text{-}o}(1\text{-}\tau_i/\tau_o)$ (days)
1.0	0.100	2500		
0.6	0.251	1200	550	1.3
0.3	0.501	700	190	1.0

Table 4 – Reaction time τ for EFA cenospheres and solid spheres (pOH = 0.3, T = 40°C) assuming $\overline{x_S} / x_{Si} = 1$ and $\overline{x_S} / x_{So} = 1$

sphere	τ_o (days)	τ_i (days)	$t_{i\text{-}o}(1\text{-}\tau_i/\tau_o)$ (days)
ceno	1000	180	1.1
solid	750	275	1.6

Table 5 – Reaction time τ for LM cenospheres and solid spheres (pOH = 0.3, T = 40°C) assuming $\overline{x_S} / x_{Si} = 1$ and $\overline{x_S} / x_{So} = 1$

sphere	τ_o (days)	τ_i (days)	$t_{i\text{-}o}(1\text{-}\tau_i/\tau_o)$ (days)
ceno	900	190	1.2
solid	700	190	1.0

Table 6 – Reaction time τ for EFA solid spheres for various temperatures (pOH = 0.3) assuming $\overline{x_S} / x_{Si} = 1$ and $\overline{x_S} / x_{So} = 1$

T (K)	τ_o (days)	τ_i (days)	$t_{i\text{-}o}(1\text{-}\tau_i/\tau_o)$ (days)
293	8000		
303	3000		
313	750	275	1.6

Table 7 – Reaction time τ for LM solid spheres for various temperatures (pOH = 0.3) assuming $\overline{x_S} / x_{Si} = 1$ and $\overline{x_S} / x_{So} = 1$

T (K)	τ_o (days)	τ_i (days)	$t_{i\text{-}o}(1\text{-}\tau_i/\tau_o)$ (days)
293	2000		
303	1500	900	1.0
313	700	190	1.0

(Tables 2, 3, 6 and 7). Moreover, the inner region appears to be more reactive that the outer region ($\tau_i < \tau_o$). Both for the ceno and solid spheres of both LM and EFA fly ash and for all temperatures and pOH, the reactivity of the inner region is about 2-5 times the reactivity of the outer region (Tables 4 and 5). Moreover, it seems that for the LM fly ash the inner region of both cenospheres and solid spheres have the same reactivity. For both EFA and LM fly ash the outer region of cenospheres is less reactive than the outer region of solid spheres.

In order to investigate the dependence of τ against the hydroxide content, in Tables 2 and 3 also [OH^-] has been included, which directly follows from the pOH. Subsequently, in Figs. 9 and 10, τ^{-1} has been set out against [OH^-] pertaining to the outer region of EFA and LM, respectively. For LM (Fig. 10) also τ^{-1} has been set out for the inner region, as two values are listed in Table 3.

From both figures one might conclude that τ, for the outer region, depends linearly on [OH^-], or is a power of [OH^-]. Accordingly, the following function has been fitted in through the inner and out region τ^{-1} (Figs. 9 and 10):

$$\tau^{-1} = b\,[OH^-]^a \qquad (33)$$

with b = 0.0026 (mole/l)$^{-a}$s^{-1} and a = 0.9 (EFA outer region), b = 0.0030 (mole/l)$^{-a}$s^{-1} and a = 1 (LM outer region) and b = 0.0140 (mole/l)$^{-a}$s^{-1} and a = 1.4 (LM inner region).

The dissolution process seems to have a direct and positive relation with [OH^-]. Song and Jennings [7] found

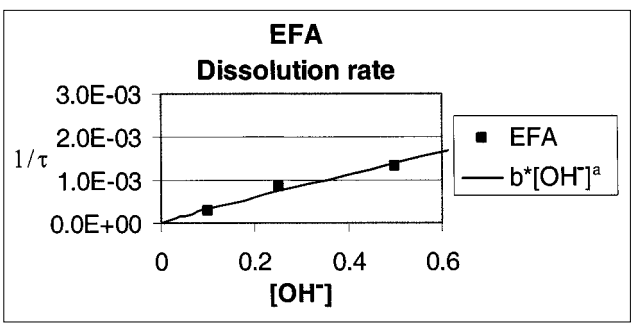

Fig. 9 – Reaction time τ against [OH^-] for EFA solid spheres (T = 40°C).

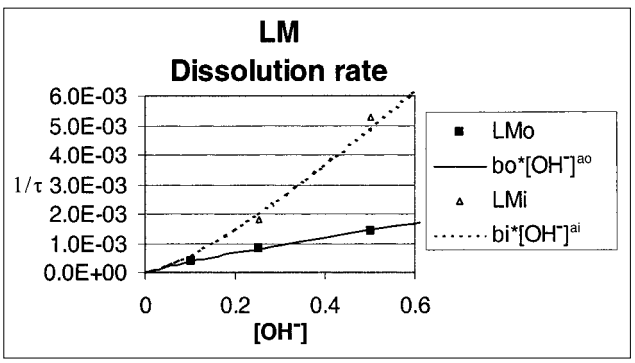

Fig. 10 – Reaction time τ against [OH^-] for LM solid spheres (T = 40°C).

a similar dependence for dissolution of slags: their measured dissolution was proportional to 10^{apH} (with a ranging from 0.97 to 1.60), which corresponds to Equation (33). Slags contain the same glass components as fly ashes, but usually in different quantities (slags are usually richer in CaO).

6. CONCLUSIONS

Pietersen [1, 2] has carefully executed and reported dissolution experiments of several types of pulverised powder coal (class F) fly ashes. To this end, the silica release in time was measured for various pOH and temperatures. In order to understand the dissolution and reaction behaviour of these fly ashes, in particular the EFA and LM fly ash, a theoretical study has been executed and the results applied to said experiments.

From the present analysis one can confirm that the available amount of reactive fly ash is proportional to the glass (non-crystalline) part of the fly ash. Moreover, as the crystalline part forms a connected network, dissolution rates are also proportional to the glass content, especially while the effective diffusion coefficient is proportional to the square of the glass content (Equation (2)).

The derivation of an extended shrinking core model yields analytical equations that reckon with a hollow core, as well as the possibility of two regions with different composition and reactivity. In Fig. 8 the shrinking behaviour in case of a more and less reactive outer region has been depicted. Application of the derived equations to the experiments of Pietersen [1, 2] provides values of the reactivity time τ (Equation (10)) for inner and outer region (τ_i and τ_o). Assuming a homogeneous silica distribution over the fly ash particle, the application reveals that the inner region is more reactive, and that about 7% and 9% of the silica is found in the outer region of LM and EFA solid spheres, respectively. From the fitting it also follows that the outer region of solid spheres and cenospheres have nearly the same thickness (about 2 μm). After dissolution of this layer, which needs less time in case of higher pH and/or temperature, the dissolution of the inner region at a higher rate starts.

The experimental application indicate a dissolution rate proportional to $[OH^-]^{0.9\text{-}1}$ for the outer region (EFA and LM), and to $[OH^-]^{1.4}$ in inner region (information available about LM only).

REFERENCES

[1] Pietersen, H. S., 'Reactivity of fly ash at high pH', Proceedings of Mat. Res. Soc. Symp. 178 (Materials Research Society, 1990) 139-157.

[2] Pietersen, H. S., 'Reactivity of fly ash and slag in cement', Ph.D. Thesis (Delft University of Technology, Delft, 1993).

[3] Fraay, A. L. A., Bijen, J. M. and De Haan, Y. M., 'The reaction of fly ash in concrete, a critical examination', *Cement and Concrete Res.* **19** (1989) 235-246.

[4] Xu, A. and Sarkar, S. L., 'Microstructural development in high-volume fly-ash cement system', *J. of Mat. in Civil Eng.* **6** (1994) 117-136.

[5] Taylor, H. F. W., 'Cement chemistry', 2nd Edn. (Thomas Telford, London, 1997).

[6] Hewlett, P. C., 'Lea's chemistry of cement and concrete', 4th Edn (Arnold, London, 1998).

[7] Song, S. and Jennings, H. M., 'Pore solution chemistry of alkali-activated ground granulated blast-furnace slag', *Cement and Concrete Res.* **29** (1999) 159-170.

[8] Song, S., Sohn, D., Jennings, H. M. and Mason, T. O., 'Hydration of alkali-activated ground granulated blast furnace slag', *J. of Mat. Sci.* **35** (2000) 249-257.

[9] Yagi, S. and Kunii, D., 'Studies on combustion of carbon particles in flames and fluidized beds', Proceedings 5th Int. Symp. on Combustion, 1955.

[10] Pietersen, H. S., private communications (2000).

[11] Hulett, L. D. and Weinberger A. J., 'Some etching studies of the microstructure and composition of large aluminosilicate particles in fly ash from coal-burning power plants', *Env. Sci. and Technology* **14** (1980) 965-970.

[12] Hemmings, R. T. and Berry, E. E., 'On the glass in coal fly ashes: recent advances', Proceedings of Mat. Res. Soc. Symp. 113 (Materials Research Society, 1988) 3- 28.

[13] Levenspiel, O., 'Chemical Reaction Engineering', 3rd Edn. (John Wiley, New York, 1999).

[14] Paul, A., 'Chemical durability of glasses; a thermodynamic approach', *J. of Mat. Sci.* **12** (1977) 2246-2268.

[15] Paul, A., 'Chemistry of Glass', 2nd Edn. (Chapman, London, 1990).

[16] Helfferich, F. G., 'Ion exchange' (Dover, New York, 1995).

[17] Dullien, F. A. L., 'Porous media: fluid transport and pore structure' (Academic Press, New York, 1979).

[18] Wakao, N. and Smith, J. M., 'Diffusion in catalyst pellets', *Chem. Eng. Sci.* **17** (1962) 825-834.